
DETRPose: Real-time end-to-end transformer model for multi-person pose estimation

Sebastian Janampa, Marios Pattichis

Department of Electrical & Computer Engineering
 The University of New Mexico
 {sebasjr1966, pattichi}@unm.edu

Abstract

Multi-person pose estimation (MPPE) estimates keypoints for all individuals present in an image. MPPE is a fundamental task for several applications in computer vision and virtual reality. Unfortunately, there are currently no transformer-based models that can perform MPPE in real time. The paper presents a family of transformer-based models capable of performing multi-person 2D pose estimation in real-time. Our approach utilizes a modified decoder architecture and keypoint similarity metrics to generate both positive and negative queries, thereby enhancing the quality of the selected queries within the architecture. Compared to state-of-the-art models, our proposed models train much faster, using 5 to 10 times fewer epochs, with competitive inference times without requiring quantization libraries to speed up the model. Furthermore, our proposed models provide competitive results or outperform alternative models, often using significantly fewer parameters. Code is available at <https://github.com/SebastianJanampa/DETRPose>

1 Introduction

Multi-person pose estimation (MPPE) estimates human keypoints from all individuals present in an image. MPPE is a fundamental problem in computer vision as a required component in larger systems that involve human interaction, activity recognition, 2D-to-3D human pose estimation, and virtual reality. Thus, fast computation of MPPE is essential for all real-time applications. Despite significant improvements in the accuracy of pose estimation models, current models can require high latency, which can hinder real-time applications.

We categorize the majority of fast MPPE methods as either top-down or bottom-up approaches. Top-down models use a pre-trained object detection to estimate bounding boxes for each human instance, followed by pose estimation for each person. Top-down models produce accurate results at the expense of slower inference, where inference time increases proportionally with the number of persons present in the image. Bottom-up methods estimate human keypoints and then assign them to groups associated with each person in the image. Compared to top-down methods, bottom-up methods tend to be much faster but less precise. The loss of precision is because the networks need to learn detection and pose estimation at the same time.

Recently, there have been efforts to adapt popular object detector frameworks (e.g., YOLO and DETR Carion et al. (2020)) to perform pose estimation. RTMO Lu et al. (2023) and YOLO11-pose Jocher and Qiu (2024) are YOLO-based models for pose estimation that achieved a good trade-off between inference speed and system precision. On the other hand, transformer-based models (e.g., DETR-based models) provided good precision while being significantly slower.

Despite progress in adapting the DETR-based model for real-time object detection, there is no real-time adaptation for pose estimation. A possible approach to speed up inference time is to employ

a light-weight encoder (e.g., see Zhao et al. (2023); Chen et al. (2024); Robinson et al. (2025)). Unfortunately, slower-inference time for DETR pose estimation is primarily due to the decoder, not the encoder. Unlike object detection, where queries are used for estimating bounding boxes for an object instance, for pose estimation, each query estimates a single keypoint associated with each person present in the image. Thus, for pose estimation, it is not clear how to benefit from speedups that focused on the decoder, the loss function, or denoising training Zhao et al. (2023); Peng et al. (2024); Shihua Huang and Shen (2025); Zhang et al. (2022) when these approaches are designed explicitly for estimating bounding boxes for object detection tasks.

In this paper, we design and present the first real-time end-to-end transformer-based pose estimation method named DETRPose. DETRPose demonstrates the adaptation of DETR for real-time pose estimation by modifying the decoder (major contribution), and the loss function used for training. Our approach is to modify the varifocal loss Zhao et al. (2023) and the Localization Quality Estimation (LQE) layer Peng et al. (2024) for pose estimation. We demonstrate that our approach achieves competitive accuracy results compared to several previously considered approaches while operating at low and constant latency. Overall, DETRPose-L achieves 72.5% Average Precision (mAP) on the COCO val2017 dataset with a latency of 32.5ms without the use of quantization libraries as `tensorrt`, which represents state-of-the-art results compared to other end-to-end methods. Compared to RTMO Lu et al. (2023), the latest state-of-the-art model for real-time MPPE, DETRPose-L converges at just 48 epochs, compared to 700 epochs for RTMO, at an effective speedup of $12.5\times$. In summary, our primary contributions include:

- A new denoising technique for pose estimation. Our approach uses object Keypoint Similarity (KS) loss for use with positive and negative queries.
- An auxiliary classification layer called Pose-LQE that improves performance. It's light-weight design allows to incorporate it to our model with sacrificing latency or GFLOPs.
- A new loss that uses the KS metric and the predicted score to increase the quality of the top-k selected queries.
- A modified decoder to support real-time end-to-end MPPE for transformer-based models.

2 Related Works

We categorize multi-person pose estimation methods into two main categories: (i) non-end-to-end methods, and (ii) end-to-end methods. We present example techniques for each category.

2.1 Non-End-to-End Methods

Non-end-to-end methods consist of two groups, single-stage and two-stage (top-down and bottom up). Single-stage methods directly estimate instance-aware keypoints Lu et al. (2023); Jocher and Qiu (2024); Maji et al. (2022). Two-stage approaches include top-down and bottom-up approaches. As mentioned in the introduction, top-down approaches tend to be more accurate. They perform person detection in the first stage, followed by pose estimation in the second stage. During training, top-down approaches train human detection based on the bounding box assigned to each person and then use the region within each bounding box to estimate pose. Bottom-up methods estimate all keypoints during the first stage, followed by grouping keypoints into instances during the second stage. A limitation of non-end-to-end methods comes from their use of hand-crafted processes such as Non-Maximum suppression (NMS). Furthermore, the use of two-stage processes provides strong-variability in inference time, associated with processing bounding boxes or grouping keypoints.

2.2 End-to-End Methods

Current end-to-end MPPE models avoid the use of NMS post-processing (e.g., see DETR Carion et al. (2020)). PETR Shi et al. (2022) was the first DETR-based model for pose estimation. PETR uses two decoders: the pose decoder and the joint decoder. The pose decoder coarsely detects the human instances by estimating their human poses. The joint decoder promotes interaction between keypoints of the same person for a more precise estimation. QueryPose Xiao et al. (2022) and ED-Pose Yang et al. (2023) follow the top-down approaches and add a human detector decoder. QueryPose employs two parallel branches, a bounding box detector and a pose detector. ED-Pose uses the sequential

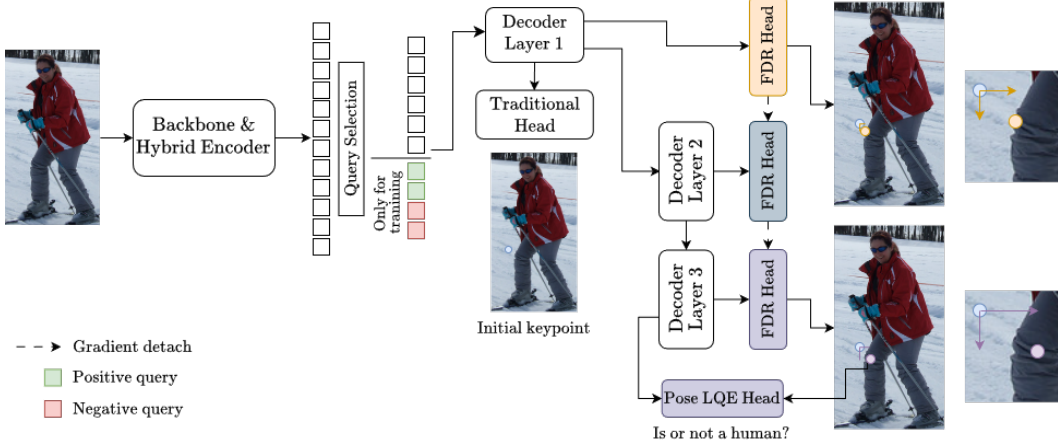


Figure 1: DETR-POSE architecture. All keypoints are estimated simultaneously. For simplicity, we present the computation for a single person. The arrows in the right-side images (knee) represent the vertical and horizontal offsets generated by the FDR heads.

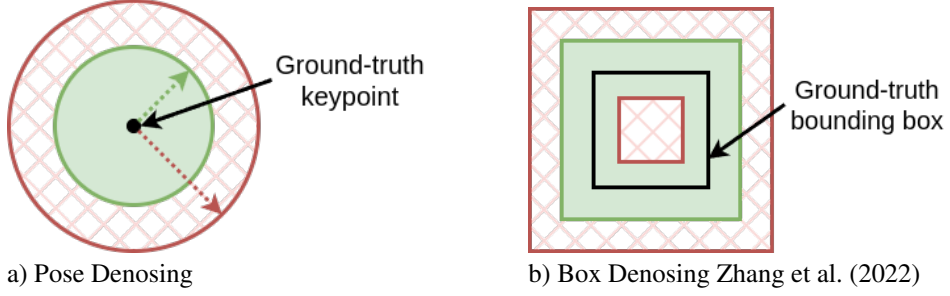


Figure 2: Denoising techniques. The right image shows the proposed pose denoising, which consists of translating the keypoints. The right image represents the box denoising (also known as contrastive denoising) from DINO Zhang et al. (2022). The positive queries will be located within the green solid area, and the negative queries will be in the red cross-hatched area.

decoder layers where the first decoder layers focus on detection and the remaining ones perform enhanced detection and pose estimation. GroupPose uses group self-attention to remove the need of detection-only decoder layers.

Although these models perform well, they do not exploit the full potential of DETR models. Except for ED-Pose, none of the models use denoising techniques developed for object detection (e.g., see Li et al. (2022); Zhang et al. (2022)). ED-Pose uses the DINO’s denoising technique Zhang et al. (2022) for the detection-only layers. In our proposed approach, DETR-Pose, we will describe a new Pose denoising technique that improves model performance without affecting inference time.

3 Methodology

We present a top-level diagram of DETR-Pose in shown in fig. 1. All keypoints are estimated simultaneously for all human instances. In this respect, DETR-Pose is similar to GroupPose. DETR-Pose uses a backbone and a hybrid encoder as input to an expanded decoder. Our backbone and hybrid encoder network is adapted for pose estimation as described by the recent D-FINE model Peng et al. (2024). The primary innovation of our approach lies in our use of Pose denoising to improve performance and substantially accelerate convergence.

3.1 Pose Denoising

We illustrate our keypoint and box denoising techniques in fig. 2. In fig. 2a, we illustrate our Pose denoising approach. For Pose denoising, we label query keypoints that fall within a small radius of the ground truth as positive. Query keypoints that fall outside are labeled as negative. In fig. 2b, we illustrate our bounding box denoising approach. For bounding box denoising, we label queries that correspond to small shifts in the corner points as positive. Otherwise, we label them as negative.

We next present a model for generating positive and negative queries for bounding box denoising. Our approach here is to consider samples generated by shifting the center and the scalings of the ground-truth bounding box. Clearly, the net effect is the same as shifting the top-left and bottom-right corners of the ground-truth bounding box. Furthermore, size changes are considered as resizing the height h and width w dimensions of the ground-truth bounding box. Let λ_{box} denote the maximum scaling factor to be applied to the ground-truth bounding box. To implement the scalings, let α_1 and α_2 be associated with random noise applied to the height and width dimensions. We assign α_1 and α_2 by taking random samples from a uniform distribution. For positive queries, we use $\alpha_1, \alpha_2 \in \mathcal{U}(-\lambda_{\text{box}}, \lambda_{\text{box}})$ where $\pm\lambda_{\text{box}}$ denote the maximum and minimum limits of the uniform distribution. We then generate positive queries by adding random noise $(\alpha_1 h, \alpha_2 w)$ to the two corners of the ground-truth bounding box. For negative queries, we sample α_1, α_2 from $\mathcal{U}(-2\lambda_{\text{box}}, -\lambda_{\text{box}}) \cup \mathcal{U}(\lambda_{\text{box}}, 2\lambda_{\text{box}})$. Here, we set $\lambda_{\text{box}} = 0.5$ to guarantee that we generate negative queries with vanishing bounding boxes as shown in fig. 2b.

We next describe our denoising approach for keypoint estimation. Our approach here is to define a similarity metric that we will use for generating positive and negative queries.

We begin by describing our similarity metric. Here, we propose an adaptive approach that is a function of the nature of the keypoint. Let i denote the index to each keypoint. Let $\kappa_i > 0$ denote a fall-off parameter that will allow us to vary our similarity metric by each keypoint. Let $0 \leq s \leq 1$ denote a scaling factor associated with each dimension. Here, we note that we normalize each keypoint coordinate to be between 0 and 1 based on $\max(w, h)$. Then, using the distance d between the ground truth and a sample keypoint, we define the object keypoint similarity (KS) using:

$$\text{KS} = \exp(-d^2/(2s^2\kappa_i^2)). \quad (1)$$

In order to derive bounds for KS, we note that the sample keypoint \hat{p} can be written as a variation of the ground truth keypoint p given by:

$$\hat{p} = p + \alpha_{\text{pose}} \vec{n} \quad (2)$$

where $\alpha_{\text{pose}} \geq 0$ is a non-fixed scaling factor and \vec{n} is a random unit vector. In order to estimate α_{pose} for generating positive and negative queries, we note that $d(p, \hat{p}) = \alpha_{\text{pose}}$, substitute it in eq. (1) to get:

$$\hat{\alpha}_{\text{pose}}^2 = -2 \ln(\text{KS}) s^2 \kappa_i^2. \quad (3)$$

Due to our use of normalized coordinates, we note that s^2 satisfies $0 \leq s^2 \leq 1$. Furthermore, to be able to take the square root of (3), we note that $0 \leq \text{KS} \leq 1$. By taking the square root of both sides of (3), we get:

$$\hat{\alpha}_{\text{pose}} = s \kappa_i \sqrt{-2 \ln(\text{KS}) w h}. \quad (4)$$

To simplify the process even further, we train DETRPose with square images. In order to generate positive and negative queries, we draw samples for KS, substitute in (3) to generate estimates for $\hat{\alpha}_{\text{pose}}$ and use a random unit vector to generate samples for \hat{p} based on (2). For positive queries, we require high similarity by sampling KS from $\mathcal{U}(0.5, 1)$. For negative queries, we require low similarity by sampling KS from $\mathcal{U}(0.1, 0.5)$.

3.2 Query Selection

We use the top-k pixels of the backbone and hybrid encoder to initialize our positional queries. DETRPose generates additional k keypoint queries based on each selected pixel. The average of all keypoints acts as an instance query. In total, we have $(k + 1)$ keypoints/positional queries for each predicted human. We also use N content queries, one per instance, as learnable queries for interaction with the feature maps, as explained next. Overall, decoder is input with $N \cdot (k + 1)$ positional queries and N content queries.

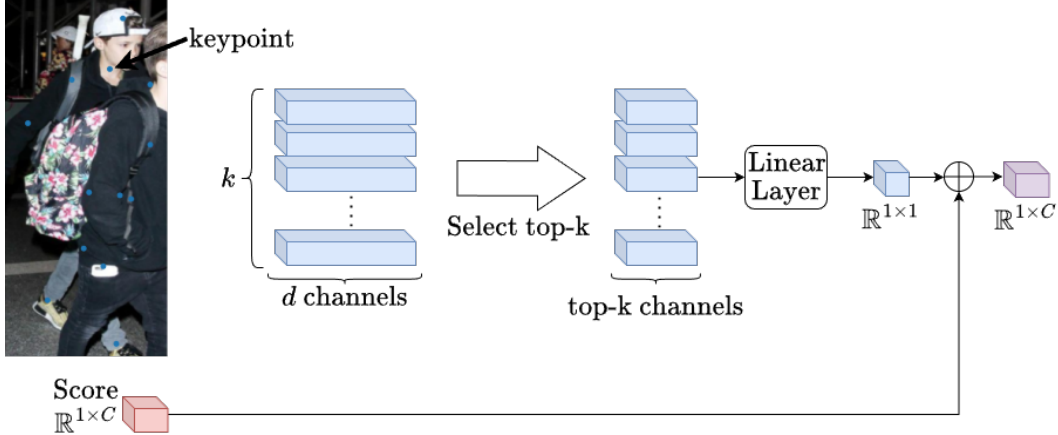


Figure 3: Pose-LQE layer for improving classification accuracy. Each keypoint is classified as either being visible or missing.

3.3 Decoder

We adopt the decoder from GroupPose. In each decoder layer, there is a within-instance self-attention layer where keypoints of the same instance interact with each other. Then, an across-instances self-attention layer promotes the interaction between keypoints of the same joint. To avoid interaction between negative, positive and prediction instances, we apply a mask attention in the across-instances self-attention layer. Next, a deformable attention mechanism supports interactions between all the queries and the enhanced feature maps.

Our decoder differs from GroupPose in two important ways. First, we add the pre-pose layer and the fine-grained distribution refinement (FDR) layers from D-FINE Peng et al. (2024). Second, we have developed the Pose localization quality estimation (LQE) layer for more precise classification whether a keypoint is visible. We will next describe the Pose-LQE layer.

3.3.1 Pose-LQE Layer

The LQE layer is a lightweight layer that refines the prediction of the classification layer using information regarding the general distribution of the bounding box provided by the FDR layers. Since DETRPose does not estimate bounding boxes, we propose a new layer, named Pose-LQE layer for estimating a bounding box for each person in the image.

Pose-LQE layer uses the predicted k keypoints for each human and extracts content information for each position from the encoder’s highest-spatial feature map as shown in fig. 3. We reduce the dimensionality of the content features by selecting the top- k values from each extracted content feature. Then a linear layer is used to process the $(\text{top-}k * k)$ values and add to the classification score extracted from the traditional classification layers.

The Pose-LQE aims to improve classification accuracy and reduce the number of queries. Here, we note that Pose-LQE does not require training on ground-truth datasets that contain segmentation masks. Instead, Pose-LQE extracts content information from a feature map located at the predicted keypoints. To speed up the process, we introduce a keypoint similarity loss that we will use to reduce the number of bounding-box queries.

3.4 Keypoint Similarity VariFocal Loss

We use the VariFocal loss to determine whether a keypoint is part of a valid member of person’s bounding box. We define the Keypoint Similarity VariFocal (KSVF) loss using:

$$\text{KSVF}(q, \tilde{c}) = \begin{cases} -q(q \log(\tilde{c}) + (1 - q) \log(1 - \tilde{c})), & q > 0 \\ -\alpha \tilde{c}^\gamma \log(1 - \tilde{c}), & q = 0 \end{cases} \quad (5)$$

Table 1: Parameter for DETRPose family.

	DETRPose-S	DETRPose-M	DETRPose-L	DETRPose-X
number of decoder layers	3	4	6	6
hidden dimension	256	256	256	384
backbone	HGNetB0	HGNetB2	HGNetB4	HGNetB5
epochs	96	60	48	48

where $q = \text{KS}$ is the keypoint similarity given in eq. (1), \tilde{c} denote the predicted classification score, α and γ are constants that control the loss function for low-similarity cases. The loss function promotes the selection of keypoints that produce a high classification score and a high similarity score.

4 Results

4.1 Datasets and DETRPose Training

We conduct experiments using the COCO Keypoints detection Lin et al. (2014) and CrowdPose Li et al. (2019) datasets. The COCO dataset has over 150K images and more than 250K person instances with 17 annotated keypoints. CrowdPose is a smaller dataset with a total of 20k images and 80K annotated human instances. CrowdPose is considered more challenging due to its crowded and occluded scenes.

We train DETRPose on the COCO train set and report results on the test – dev set. For the CrowdPose dataset, we use the trainval set for training and evaluate on the test set. We train and test using 4 Tesla V100s. For latency, we report our using TensorRTv8.6.4 FP16 a single Tesla V100.

We trained four different DETRPose models as summarized in table 1. By varying the number of trainable parameters, we developed DETRPose-S, DETRPose-M, DETRPose-L, and DETRPose-X. All the models use AdamW as an optimizer with a learning rate of 0.0001. For information about the encoder parameters, see Peng et al. (2024)

During training, we apply data augmentation that includes horizontal flipping, color jittering, mosaic composition, and multiscale sampling. To provide fair comparisons, we follow the RTMOLu et al. (2023) protocol by applying transfer learning to our backbone and encoder. As for RTMO, we use transfer learning from D-FINE Peng et al. (2024) models trained on Object365 dataset Shao et al. (2019). We train using a batch size of 16 for all models. During validation and testing, we rescale the input images to 640×640 .

4.2 Comparisons

4.2.1 COCO Dataset Comparisons

We provide comprehensive comparisons against several other methods using the COCO test-dev dataset in table 2. Among previous end-to-end models not using the Swin-L backbone, DETRPose-L gave the best results while using the lowest number of trainable parameters. When compared against non end-to-end models, we note DETRPose-L gave the second-best results, behind RTMO-L which uses significantly more parameters. Overall, we note that DETRPose-L outperforms all non end-to-end models by a margin of 0.5 in AP_L (79.9) and AR (78.1). DETRPose-X, our biggest model, gave competitive results against end-to-end models with huge backbones and large number of parameters based on Swin-L. In terms of inference speed, DETRPose-X set a new record, performing pose estimation in real-time. For results on the COCO val, see appendix A.

4.2.2 CrowdPose Dataset Comparisons

We provide comprehensive comparisons using the CrowdPose dataset in table 3. We note that the results on CrowdPose are more significant since this is a more challenging dataset. From the results, we note that DETRPose-M,L,X surpass PETR and ED-Pose by significant margins. We emphasize

Table 2: Performance comparison of state-of-the-art methods on the COCO test-dev dataset. Best and second results are in **bold** and *italic*.

Method	Backbone	#Params	Time (ms)	AP	AP ₅₀	AP ₇₅	AP _M	AP _L	AR
Non-end-to-end methods									
DirectPose Tian et al. (2019)	ResNet-50	-	74	62.2	86.4	68.2	56.7	69.8	-
DirectPose Tian et al. (2019)	ResNet-101	-	-	63.3	86.7	69.4	57.8	71.2	-
FCPose Mao et al. (2021)	ResNet-50	41.7M	68	64.3	87.3	71.0	61.6	70.5	-
FCPose Mao et al. (2021)	ResNet-101	60.5M	93	65.6	87.9	72.6	62.1	72.3	-
CID Wang and Zhang (2022)	HRNet-w32	29.4M	84.0	68.9	89.9	76.9	63.2	77.7	74.6
CID Wang and Zhang (2022)	HRNet-w48	65.4M	94.8	70.7	90.4	77.9	66.3	77.8	76.4
InsPose Shi et al. (2021)	ResNet-50	50.2M	80	65.4	88.9	71.7	60.2	72.7	-
InsPose Shi et al. (2021)	ResNet-101	-	100	66.3	89.2	73.0	61.2	73.9	-
CenterNet Zhou et al. (2019)	Hourglass	194.9M	160	63.0	86.8	69.6	58.9	70.4	-
KAPAO-S McNally et al. (2021)	CSPNet	12.6M	26.9	63.8	88.4	70.4	58.6	71.7	71.2
KAPAO-M McNally et al. (2021)	CSPNet	35.8M	37.0	68.8	90.5	76.5	64.3	76.0	76.3
KAPAO-L McNally et al. (2021)	CSPNet	77.0M	50.2	70.3	91.2	77.8	66.3	76.8	77.7
YOLO-Pose-s Maji et al. (2022)	CSPDarknet	10.8M	7.9	63.2	87.8	69.5	57.6	72.6	67.6
YOLO-Pose-m Maji et al. (2022)	CSPDarknet	29.3M	12.5	68.6	90.7	75.8	63.4	77.1	72.8
YOLO-Pose-l Maji et al. (2022)	CSPDarknet	61.3M	20.5	70.2	91.1	77.8	65.3	78.2	74.3
RTMO-r50 Lu et al. (2023)	ResNet-50	41.7M	15.5	70.9	91.0	78.2	65.8	79.1	75.0
RTMO-S Lu et al. (2023)	CSPDarknet	9.9M	8.9	66.9	88.8	73.6	61.1	75.7	70.9
RTMO-M Lu et al. (2023)	CSPDarknet	22.6M	12.4	70.1	90.6	77.1	65.1	78.1	74.2
RTMO-L Lu et al. (2023)	CSPDarknet	44.8M	19.1	71.6	91.1	79.0	66.8	79.1	75.6
End-to-end methods with Swin-L backbone									
ED-Pose Yang et al. (2023)	Swin-L	218.0M	222.6	72.7	92.3	80.9	67.6	80.0	-
QueryPoseXiao et al. (2022)	Swin-L	-	-	73.3	91.3	79.5	68.5	81.2	-
PETR Shi et al. (2022)	Swin-L	213.8M	133	70.5	91.5	78.7	65.2	78.0	-
GroupPose Liu et al. (2023)	Swin-L	219.6M	214.0	74.8	91.6	82.1	69.4	83.0	-
End-to-end methods									
ED-Pose Yang et al. (2023)	ResNet-50	50.6M	125.5	69.8	90.2	77.2	64.3	77.4	-
PETR Shi et al. (2022)	ResNet-50	43.7M	89	67.6	89.8	75.3	61.6	76.0	-
QueryPoseXiao et al. (2022)	ResNet-50	-	-	68.7	88.6	74.4	63.8	76.5	-
GroupPose Liu et al. (2023)	ResNet-50	52.4M	116.5	70.2	90.5	77.8	64.7	78.0	-
DETRPose-S (ours)	HGNetv2-B0	11.9M	20.3	66.5	87.4	72.5	59.8	76.8	73.0
DETRPose-M (ours)	HGNetv2-B2	23.5M	25.8	68.5	88.6	74.6	62.1	78.3	74.6
DETRPose-L (ours)	HGNetv2-B4	36.8M	32.5	71.2	91.2	78.1	65.8	79.9	78.1
DETRPose-X (ours)	HGNetv2-B5	82.3M	52.1	72.2	91.4	79.3	67.0	80.6	78.8

that DETRPose-M uses only 24M parameters which is $8\times$ less than models based on the Swin-L backbone. DETRPose models outperform their RTMO counterparts (S, M, L models).

DETRPose is significantly faster to train than RTMO. DETRPose-S requires 150 epochs to achieve competitive results. DETRPose-X only needs 80 epochs. RTMO models require 800 epochs which is $5.3\times$ than what is needed for DETRPose-S and $10\times$ more than what is needed for DETR-X.

DETRPose-X set a new state-of-the-art record for real-time MPPE models with a score of 75.1 for the AP metric. Overall, DETRPose-X surpasses all other models except for ED-Pose[†]. In terms of parameters, ED-Pose uses 218M versus 82.3M for DETERPose-X. ED-Pose is also significantly slower and not suitable for real-time pose estimation applications. Clearly, DETRPose-X provides strong evidence that our proposed transformer-based methods hold great promise for multi-person pose estimation.

4.3 Ablation study

We provide a step-by-step analysis for each proposed component in DETRPose. For this study, we use the COCO val dataset to report results. For each step, we train DETRPose-L on the COCO train set for 12 epochs. To start our study, we create RT-GroupPose, which consist on adding the D-FINE’s backbone and encoder to the original GroupPose. We use RT-GroupPose as a baseline. We observe that reducing the number of instance queries from 100 to 60 reduces the AP score by 0.5, but it also reduces the GFLOPs. Next, we observe using our proposed Pose Denoising helps the model to achieve an AP score of 62.8. Since this is a training strategy, it does not have any effect during inference. Then, we add the FDR head to boost performance. We get an increment of 1.6 points in the AP score, and the GFLOPS also increases 4 unit. The addition of the KSVF loss produces a drop in the AP metric. This occurs because the predicted keypoints and confidence scores do not come

Table 3: Performance comparison of state-of-the-art on the CrowdPose **test** dataset. The symbol \dagger means the full model is trained with additional data beyond the COCO **train2017** dataset. Best and second results are in **bold** and *italic*.

Method	Backbone	AP	AP ₅₀	AP ₇₅	AP _E	AP _M	AP _H
Non-end-to-end methods							
RTMO-S Lu et al. (2023)	CSPDarknet	67.3	88.2	72.9	73.7	68.2	59.1
RTMO-M Lu et al. (2023)	CSPDarknet	71.1	87.7	77.1	77.4	71.9	63.4
RTMO-L Lu et al. (2023)	CSPDarknet	73.2	90.7	79.3	79.2	74.1	65.3
End-to-end methods with Swin-L backbone							
PETR Shi et al. (2022)	Swin-L	71.6	90.4	78.3	77.3	72.0	65.8
QueryPoseXiao et al. (2022)	Swin-L	72.7	91.7	78.1	79.5	73.4	65.4
ED-Pose Yang et al. (2023)	Swin-L	73.1	90.5	79.8	80.5	73.8	63.8
ED-Pose [†] Yang et al. (2023)	Swin-L	76.6	92.4	83.3	83.0	77.3	68.3
GroupPose Liu et al. (2023)	Swin-L	74.1	91.3	80.4	80.8	74.7	66.4
End-to-end methods							
PETR Shi et al. (2022)	ResNet-50	68.8	87.5	76.3	62.7	77.7	-
ED-Pose Yang et al. (2023)	ResNet-50	69.9	88.6	75.8	77.7	70.6	60.9
DETRPose-S (ours)	HGNetv2-B0	67.4	88.6	72.9	74.7	68.1	5.93
DETRPose-M (ours)	HGNetv2-B2	72.0	91.0	77.8	78.6	72.6	64.5
DETRPose-L (ours)	HGNetv2-B4	73.3	91.6	79.4	79.5	74.0	66.1
DETRPose-X (ours)	HGNetv2-B5	75.1	92.1	81.3	81.3	75.7	68.1

Table 4: Step-by-step modifications from baseline to DETRPose-L. Each step shows the AP, number of parameters, and the GFLOPs.

Model	AP	#Params	GFLOPs
baseline: RT-GroupPose	61.2	34.9M	115.2
Reducing number of instance queries (100 \rightarrow 60)	60.7	34.8M	103.3
+ Pose Denoising Technique	62.8	34.8M	103.3
+ FDR Heads	64.4	36.7M	107.2
+ KSVF loss	63.5	36.7M	107.2
+ Pose-LQE Head	65.7 (\uparrow 7.4%)	36.8M	107.2
+ Transfer Learning	67.5 (\uparrow 10.3%)	36.8M (\uparrow 5.4%)	107.2 (\downarrow 5%)

from the same query as in object detection. To address that, we add a new classification head called Pose-LQE. This head promotes the interaction between the predicted keypoints and the confidence score allowing different type of queries to interact between each other. The addition of this is highly beneficial as it produces an AP of 65.7 points. Finally, we use transfer learning in the encoder and backbone to improve results. At the end, we observed that all our modifications together produce an increment of 10.3% in AP score. For the parameters, there is a small increment of 5%. Nevertheless, we decreased the GFLOPs by 10%.

5 Conclusion

In this paper, we have presented a new real-time end-to-end pose estimator. DETRPose does not only produce new-state-of-the-art result but also has faster convergence. Results on multiple datasets show that DETRPose great results and prove that DETR-based models can be adapted for pose estimation showing a future for DETR models in MPPE task.

Acknowledgment

This work was supported in part by the National Science Foundation under Grant 1949230, Grant 1842220, and Grant 1613637, and by Lambda.ai.

References

Nicolas Carion, Francisco Massa, Gabriel Synnaeve, Nicolas Usunier, Alexander Kirillov, and Sergey Zagoruyko. End-to-end object detection with transformers. In *Proceedings of the European Conference on Computer Vision*, pages 213–229, 2020.

Qiang Chen, Xiangbo Su, Xinyu Zhang, Jian Wang, Jiahui Chen, Yunpeng Shen, Chuchu Han, Ziliang Chen, Weixiang Xu, Fanrong Li, et al. Lw-detr: A transformer replacement to yolo for real-time detection. *arXiv preprint arXiv:2406.03459*, 2024.

Glenn Jocher and Jing Qiu. Ultralytics yolo11, 2024.

Glenn Jocher, Ayush Chaurasia, and Jing Qiu. Ultralytics yolov8, 2023.

Feng Li, Hao Zhang, Shilong Liu, Jian Guo, Lionel M Ni, and Lei Zhang. Dn-detr: Accelerate detr training by introducing query denoising. In *Proceedings of the IEEE/CVF Conference on Computer Vision and Pattern Recognition*, pages 13619–13627, 2022.

Jiefeng Li, Can Wang, Hao Zhu, Yihuan Mao, Hao-Shu Fang, and Cewu Lu. Crowdpose: Efficient crowded scenes pose estimation and a new benchmark. In *Proceedings of the IEEE/CVF Conference on Computer Vision and Pattern Recognition*, pages 10863–10872, 2019.

Tsung-Yi Lin, Michael Maire, Serge Belongie, James Hays, Pietro Perona, Deva Ramanan, Piotr Dollár, and C Lawrence Zitnick. Microsoft coco: Common objects in context. In *Proceedings of the European Conference on Computer Vision*, pages 740–755, 2014.

Huan Liu, Qiang Chen, Zichang Tan, Jiangjiang Liu, Jian Wang, Xiangbo Su, Xiaolong Li, Kun Yao, Junyu Han, Errui Ding, Yao Zhao, and Jingdong Wang. Group pose: A simple baseline for end-to-end multi-person pose estimation. In *Proceedings of the IEEE International Conference on Computer Vision (ICCV)*, 2023.

Peng Lu, Tao Jiang, Yining Li, Xiangtai Li, Kai Chen, and Wenming Yang. RTMO: Towards high-performance one-stage real-time multi-person pose estimation, 2023.

Debapriya Maji, Soyeb Nagori, Manu Mathew, and Deepak Poddar. Yolo-pose: Enhancing yolo for multi-person pose estimation using object keypoint similarity loss. In *Proceedings of the IEEE/CVF conference on computer vision and pattern recognition*, pages 2637–2646, 2022.

Weian Mao, Zhi Tian, Xinlong Wang, and Chunhua Shen. Fcpose: Fully convolutional multi-person pose estimation with dynamic instance-aware convolutions. In *Proceedings of the IEEE/CVF Conference on Computer Vision and Pattern Recognition*, pages 9034–9043, 2021.

William McNally, Kanav Vats, Alexander Wong, and John McPhee. Rethinking keypoint representations: Modeling keypoints and poses as objects for multi-person human pose estimation. *arXiv preprint arXiv:2111.08557*, 2021.

Yansong Peng, Hebei Li, Peixi Wu, Yueyi Zhang, Xiaoyan Sun, and Feng Wu. D-fine: Redefine regression task in detrs as fine-grained distribution refinement, 2024.

Isaac Robinson, Peter Robicheaux, and Matvei Popov. Rf-detr. <https://github.com/roboflow/rf-detr>, 2025. SOTA Real-Time Object Detection Model.

Shuai Shao, Zeming Li, Tianyuan Zhang, Chao Peng, Gang Yu, Jing Li, Xiangyu Zhang, and Jian Sun. Objects365: A large-scale, high-quality dataset for object detection. In *Proceedings of the IEEE/CVF International Conference on Computer Vision*, pages 8425–8434, 2019.

Dahu Shi, Xing Wei, Xiaodong Yu, Wenming Tan, Ye Ren, and Shiliang Pu. Inspose: instance-aware networks for single-stage multi-person pose estimation. In *Proceedings of the 29th ACM International Conference on Multimedia*, pages 3079–3087, 2021.

Dahu Shi, Xing Wei, Liangqi Li, Ye Ren, and Wenming Tan. End-to-end multi-person pose estimation with transformers. In *Proceedings of the IEEE/CVF Conference on Computer Vision and Pattern Recognition*, pages 11069–11078, 2022.

Xiaodong Cun, Yongjun Yu, Xiao Zhou, Shihua Huang, Zhichao Lu, and Xi Shen. Deim: Detr with improved matching for fast convergence, 2025.

Zhi Tian, Hao Chen, and Chunhua Shen. Directpose: Direct end-to-end multi-person pose estimation. *arXiv preprint arXiv:1911.07451*, 2019.

Dongkai Wang and Shiliang Zhang. Contextual instance decoupling for robust multi-person pose estimation. In *Proceedings of the IEEE/CVF Conference on Computer Vision and Pattern Recognition (CVPR)*, pages 11060–11068, 2022.

Yabo Xiao, Kai Su, Xiaojuan Wang, Dongdong Yu, Lei Jin, Mingshu He, and Zehuan Yuan. Querypose: Sparse multi-person pose regression via spatial-aware part-level query. In *Advances in Neural Information Processing Systems*, pages 1–14, 2022.

Jie Yang, Ailing Zeng, Shilong Liu, Feng Li, Ruimao Zhang, and Lei Zhang. Explicit box detection unifies end-to-end multi-person pose estimation. In *International Conference on Learning Representations*, pages 1–17, 2023.

Hao Zhang, Feng Li, Shilong Liu, Lei Zhang, Hang Su, Jun Zhu, Lionel Ni, and Harry Shum. Dino: Detr with improved denoising anchor boxes for end-to-end object detection. In *International Conference on Learning Representations*, pages 1–18, 2022.

Yian Zhao, Wenyu Lv, Shangliang Xu, Jinman Wei, Guanzhong Wang, Qingqing Dang, Yi Liu, and Jie Chen. Detrs beat yolos on real-time object detection, 2023.

Xingyi Zhou, Dequan Wang, and Philipp Krähenbühl. Objects as points. *arXiv preprint arXiv:1904.07850*, 2019.

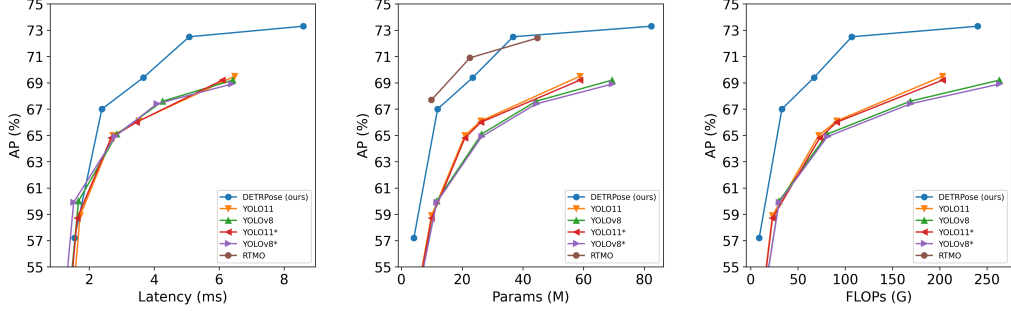


Figure 4: Comparisons with other pose estimation models in terms of latency (left), model size (mid), and computational cost (right). We measure end-to-end latency using TensorRTv10.11 FP16 on an NVIDIA A10 GPU.

A COCO val comparison

We provide comparisons against YOLO-based methods on the COCO val dataset and report the results in table 5 and fig. 4. We run the experiments on a Nvidia A100 using Lambda.ai¹ instance. We use TensorRT 10.11 with FP16 to report the inference time. The reason of our choice is to compare against YOLOv8 and YOLOv11 since those models can not be exported to TensorRT 8.6.4.

We observe that DETRPose provides the two best results for all metrics except AP₅₀. At first sight, DETRPose is slower than any of its YOLO counterparts, especially for the X and L versions. Nevertheless, notice that DETRPose-M surpasses all YOLO-based models except for YOLOv11-X, but only for 0.1 points. This result shows the efficiency of our model in estimating keypoints.

Table 5: Performance comparison of state-of-the-art one-stage methods on the COCO val dataset. Best and second results are in **bold** and *italic*.

Method	#Params	Time (ms)	GFLOPs	AP	AP ₅₀	AP ₇₅	AP _M	AP _L	AR
Non-end-to-end methods									
YOLOv8-N Jocher et al. (2023)	3.3M	1.30	9	50.4	80.0	54.1	43.1	62.2	57.8
YOLOv8-S Jocher et al. (2023)	11.6M	1.67	30	60.0	86.2	65.9	53.8	70.2	66.7
YOLOv8-M Jocher et al. (2023)	26.4M	2.85	81	65.1	88.8	72.2	60.5	73.6	71.8
YOLOv8-L Jocher et al. (2023)	44.4M	4.26	169	67.6	90.0	74.6	63.3	75.7	74.2
YOLOv8-X Jocher et al. (2023)	69.4M	6.42	263	69.2	90.2	76.6	65.4	76.7	75.7
YOLOv8-N* Jocher et al. (2023)	3.3M	1.17	9	50.4	79.8	54.0	43.1	62.1	57.4
YOLOv8-S* Jocher et al. (2023)	11.6M	1.52	30	59.9	85.8	65.9	53.7	70.1	66.3
YOLOv8-M* Jocher et al. (2023)	26.4M	2.79	81	64.9	88.8	72.2	60.4	73.4	71.4
YOLOv8-L* Jocher et al. (2023)	44.4M	4.08	169	67.4	89.6	74.6	63.2	75.5	73.8
YOLOv8-X* Jocher et al. (2023)	69.4M	6.38	263	68.9	89.7	76.6	65.1	76.5	75.2
YOLO11-N Jocher and Qiu (2024)	2.9M	1.41	8	50.0	80.6	53.4	43.6	60.9	57.7
YOLO11-S Jocher and Qiu (2024)	9.9M	1.72	23	58.9	86.2	64.8	54.0	67.9	66.1
YOLO11-M Jocher and Qiu (2024)	20.9M	2.73	72	65.0	89.3	72.3	62.3	71.1	72.2
YOLO11-L Jocher and Qiu (2024)	26.2M	3.53	91	66.1	90.0	73.6	63.2	73.1	73.3
YOLO11-X Jocher and Qiu (2024)	58.8M	6.48	203	69.5	91.2	77.4	66.6	76.0	76.3
YOLO11-N* Jocher and Qiu (2024)	2.9M	1.31	8	49.8	80.6	53.2	43.5	60.8	57.2
YOLO11-S* Jocher and Qiu (2024)	9.9M	1.63	23	58.7	85.9	64.5	53.8	67.8	65.6
YOLO11-M* Jocher and Qiu (2024)	20.9M	2.67	73	64.8	89.3	72.0	62.1	71.5	71.7
YOLO11-L* Jocher and Qiu (2024)	26.2M	3.45	91	66.0	89.6	73.3	63.1	72.9	72.9
YOLO11-X* Jocher and Qiu (2024)	58.8M	6.10	203	69.2	90.7	76.9	66.5	75.9	75.9
RTMO-S Lu et al. (2023)	9.9M	-	-	67.7	87.8	73.7	-	-	71.5
RTMO-M Lu et al. (2023)	22.6M	-	-	70.9	89.0	77.8	-	-	74.7
RTMO-L Lu et al. (2023)	44.8M	-	-	72.4	89.9	78.8	-	-	76.2
End-to-end methods									
DETRPose-N (ours)	4.1M	1.55	9	57.2	81.7	61.4	48.2	70.5	64.4
DETRPose-S (ours)	11.9M	2.39	33	67.0	87.6	72.8	60.2	77.4	73.5
DETRPose-M (ours)	23.5M	3.67	67	69.4	89.2	75.4	63.2	79.0	75.5
DETRPose-L (ours)	36.8M	5.08	107	72.5	90.6	79.0	66.3	82.2	78.7
DETRPose-X (ours)	82.3M	8.59	240	73.3	90.5	79.4	67.5	82.7	79.4

¹<https://lambda.ai>

B Limitations

Table 5 shows that DETRPose has equal or less GFLOPS than YOLOv8, but it has a higher latency. A possible reason of this is the largely use of the transpose operation producing non-continuous vectors and therefore the time to access elements.

Since DETRPose is built on GroupPose, our model does not estimates bounding boxes, therefore, it can not be directly use for object tracking. Another limitation from DETRPose and previous transformer-based pose estimation models is that transformer models do not determine if the keypoint is visible or not.